Spatial heterogeneity and the stability of reaction states in autocatalysis

Glenn Marion*
Biomathematics & Statistics Scotland, James Clerk Maxwell Building, The King's Buildings, Mayfield Road, Edinburgh EH9 3JZ, United Kingdom

Xuerong Mao and Eric Renshaw
Department of Statistics & Modelling Science, University of Strathclyde, Glasgow G1 1XH, United Kingdom

Junli Liu
Computational Biology Programme, Scottish Crop Research Institute, Invergowrie, Dundee DD2 5DA, United Kingdom
(Received 14 March 2002; revised manuscript received 5 July 2002; published 22 November 2002)

The impact of stochasticity and spatial heterogeneity on the quadratic autocatalytic system is studied. In a nonspatial setting the reactive state of the system is found to be unstable in small volumes where internal fluctuations drive the system to the unreactive state. This phenomena is of potential importance to the stability of reactions in biological cells. A simple spatial model is constructed by linking N nonspatial models via migration of reactants controlled by a mixing rate λ. Simulation of this stochastic process demonstrates the importance of such mixing in controlling the impact of internal fluctuations on the stability of the autocatalytic reaction. For high mixing rate the mean reactant levels in equilibrium correspond to the well-mixed deterministic system, although a significant degree of spatial heterogeneity remains. For intermediate mixing rates, mean reactant levels vary continuously with λ, where the interaction of internal fluctuations with limited spatial mixing modifies the reactive states of the deterministic system. However, there is a threshold below which mixing is unable to control internal fluctuations which drive the system into the unreactive state. Thus a critical minimum level of communication between the cells is required to stabilize the reaction across the entire system. Approximate analytic results, obtained using moment-closure techniques, support these findings and demonstrate the relationship between the spatial stochastic and nonspatial deterministic models.

DOI: 10.1103/PhysRevE.66.051915 PACS number(s): 82.39.−k, 82.20.−w, 02.50.−r

I. INTRODUCTION

In the absence of macroscopic environmental fluctuations, classical reaction kinetics applies ordinary differential equations to describe the progress of reactions in large volumes under conditions of perfect mixing. However, in many biochemical systems reactions occur in minute volumes and both stochasticity and spatial heterogeneity play important roles in living cells. For example, by reference to cell volume, Gibson and Bruck [1] show that the number of protein molecules involved in reactions controlling gene regulation in the Lambda phage infection of *Escherichia coli* is of the order 10–100. Moreover, the outcome of this infection process is stochastic. Autocatalytic mechanisms play an important role in the organization and coordination of biological cells, and quadratic- or cubic-autocatalysis represents generic models whose behavior in stochastic and spatially heterogeneous systems are important for understanding processes in living cells. This paper addresses these issues by exploring the impact of stochasticity and spatial heterogeneity in the quadratic autocatalytic process

$$A+B\rightarrow 2B,\quad B\rightarrow C,$$

where a B-particle catalyses the conversion of reactant A into further B's, and reactant B also decays to product C [2,3]. Positive feedback is seen as a central mechanism in many important biochemical processes such as glycolysis [4]; autocatalytic systems of this type have been widely studied as prototypical feedback systems [2,3,5,6]. Horsthemke and Lefever [7] study the effect of environmental noise on a range of one-dimensional dynamical systems, and find that stochasticity may radically alter the behavior of deterministic models, for example, by inducing transitions between steady states of the deterministic system, altering the level of such states, or by inducing new states. Marion *et al.* [8] study the effect of both environmental and internal noise on the quadratic autocatalytic processes in the nonspatial setting of a continuous-flow stirred tank reactor (CSTR), whilst the present paper focuses on the role of internal fluctuations in a spatially extended system. First, however, we review the behavior of the nonspatial process.

When quadratic autocatalysis is carried out in a CSTR, the system can be considered to be well mixed, of large volume, and adequately described by the deterministic model

$$\begin{aligned} d\alpha(t)/dt&=[\alpha_0-\alpha(t)]\nu-\kappa\alpha(t)\beta(t),\\ d\beta(t)/dt&=\kappa\alpha(t)\beta(t)-(K_b+\nu)\beta(t), \end{aligned} \tag{1}$$

where $\alpha(t)$ and $\beta(t)$ represent the concentrations of A and B particles, respectively. Reactant A is supplied at rate $\nu\alpha_0$ from a reservoir of fixed concentration α_0: both A and B are removed from the reaction vessel at rates $\nu\alpha$ and $\nu\beta$, respectively. The decay $B\rightarrow C$ occurs at rate $K_b\beta$, and the name of the process derives from the quadratic rate, $\kappa\alpha\beta$,

*Email address: glenn@bioss.ac.uk

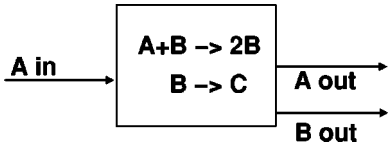

FIG. 1. Schematic representation of a nonspatial model of the autocatalytic process.

for the autocatalytic step $A+B\rightarrow 2B$. This system has two fixed points, the *reactive state* (α_1,β_1) and the *unreactive state* (α_2,β_2) given by

$$\alpha_1=(K_b+\nu)/\kappa, \quad \beta_1=\nu(\alpha_0\kappa-K_b-\nu)/[\kappa(K_b+\nu)]$$

$$\alpha_2=\alpha_0, \quad \beta_2=0. \tag{2}$$

Where chemical and biochemical reactions occur in small volumes, or in poorly mixed conditions, deterministic descriptions such as Eq. (1) prove inadequate, and this is particularly true at low densities where finite size effects are most significant. In such cases, discrete state-space Markov models, or birth-death processes, have been extensively used in modeling chemical reactions and a wide range of biological and physical systems. In the physicochemical literature, models of this type are said to describe the state of the system at a *mesoscopic* scale: that is, an intermediate scale between the *microscopic* scale, where molecular dynamic or even quantum mechanical descriptions should be used, and the *macroscopic* scale where (in deterministic environments) deterministic descriptions such as Eq. (1) are often employed [9]. In a general birth-death process, the probability of change of state in a small time interval $(t,t+\delta t)$ can be written as

$$P(n(t+\delta t)=n(t)+\delta n)=R(n\rightarrow n+\delta n)\,\delta t, \tag{3}$$

where the vector $\delta n=(\delta n_1,\delta n_2,\ldots)^T$ represents the change in state $n=(n_1,n_2,\ldots)^T$ which occurs at rate $R(n\rightarrow n+\delta n)$. The change δn_i in population i is an integer, and often ± 1. The fluctuations caused by the stochastic nature of the events are typically referred to as internal fluctuations in physical and chemical models, and as demographic fluctuations in biological systems. Whilst the exact simulation is straightforward, since interevent times are exponentially distributed [10], an approximate alternative approach is to update time by a sufficiently small time step δt and then to choose the event $n\rightarrow n+\delta n$ with probability (3).

To model the nonspatial (Fig. 1) quadratic autocatalytic system described above at the mesoscopic level, we write $n=(n_A,n_B)^T$ with $\delta n=(\delta n_A,\delta n_B)^T$ and the rates $R(n\rightarrow n+\delta n)$ as

Rate	δn_A	δn_B	
Kn_An_B	-1	$+1$	Autocatalytic reaction
K_bn_B	0	-1	Decay of reactant B
νn_{A0}	$+1$	0	Influx of reactant A
νn_A	-1	0	Outflow of reactant A
νn_B	0	-1	Outflow of reactant B
0	otherwise		(4)

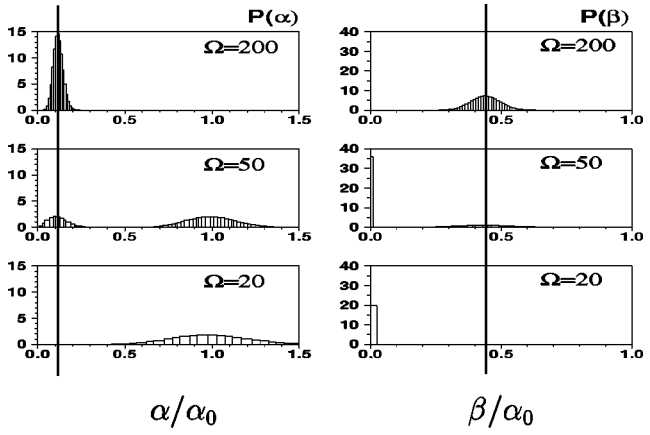

FIG. 2. The effect of volume in the nonspatial system. Histograms from simulations of the Markov processes (3) and (4), with $\alpha=n_A/\Omega$, $\beta=n_B/\Omega$, and parameter values $\kappa=1$, $\alpha_0=1$, $\nu=K_b=1/17$. Samples of the processes are taken for $t=(900\,000,1\,000\,000)$. The solid vertical lines represent the equilibrium values obtained from the deterministic model (1).

The connection with the deterministic system (1) is made by introducing the system volume Ω and writing the densities $\alpha=n_A/\Omega$ and $\beta=n_B/\Omega$, which for finite volumes are random variables. However, if the reaction rate scales $K=\kappa/\Omega$, then in the large volume limit $\Omega\rightarrow\infty$ it can be shown that α and β obey the deterministic equations (1) [8,11,12].

Figure 2 shows the effect of system volume on the stability of the reactive state. The results shown are based on simulated data collected for $t=(900\,000,1\,000\,000)$ and thus represent samples from the quasiequilibrium distribution of the birth-death processes (3) and (4). The parameter values used are $\kappa=1$, $\alpha_0=1$, $\nu=K_b=1/17$ [5]. For large volume $(\Omega=200)$ internal fluctuations induce a distribution centered on the deterministic steady state (α_1,β_1); the reactive state is stable with respect to internal fluctuations. However, for small volumes $(\Omega=20)$, the system is driven toward an unreactive state with fluctuations about the deterministic steady state (α_2,β_2). At intermediate volumes $(\Omega=50)$, the reactive state remains stable with nonzero probability, but a proportion of realizations fall into the unreactive state. Thus, for small volumes, where the reactive state is totally destabilized by internal fluctuations, there are qualitative differences between deterministic and stochastic models. Zheng *et al.* [13] study a related system in which the concentration of A particles is held fixed. The exact stationary distribution may then be calculated since the resulting system is one dimensional [10]. Zheng *et al.* show that as the system volume increases the relative heights of peaks in this distribution invert; a similar effect to that shown in Fig. 2. However, in contrast with the present case, where only one fixed point of the deterministic dynamics is attracting, these peaks are associated with two attracting steady states of the corresponding deterministic system. For cellular systems it may seem unnatural to adjust the system volume. However, the above results hold for changes in the density of reactants, with low densities corresponding to an unstable reactive state; for fixed cell volume changes in density correspond to changes

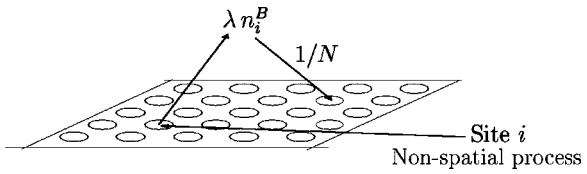

FIG. 3. Schematic representation of the spatial autocatalytic process in which N nonspatial Markov processes (3) and (4) are linked together via random migration of B particles.

in the number of reactant molecules per cell. Indeed, it has been found that in living cells the number of molecules can be very low and enzymatic reactions occur in small volumes [1,14].

In the remainder of this paper we study the effect of spatial heterogeneity on the stability of the reactive state in quadratic autocatalysis. Section II introduces a spatial autocatalytic model in which N nonspatial processes (3) and (4), each with volume $\Omega=1$, are coupled via random migration of B particles, which is controlled by a mixing rate λ. Stochastic simulation is used to explore the stability of the reactive state for a range of values of λ. Section III applies moment-closure techniques to develop approximations describing the system, they support the simulation results, reveal the relationship between the nonspatial deterministic model and the spatial stochastic system, and yield analytic insights into the system behavior in the limits of high and low mixing. Finally, in Sec. IV we discuss the relevance of our results to living cells.

II. SPATIAL PROCESS

Figure 3 depicts the spatial autocatalytic process constructed by linking N nonspatial models via the migration of B particles. The numbers of A and B particles at site $i=1,\ldots,N$ are denoted n_i^A and n_i^B, respectively. The within-site behavior is described by the nonspatial model (3) and (4), whilst the migration of B particles is described by

$$P(n_i^B(t+\delta t)=n_i^B(t)-1)=\lambda n_i^B\delta t,$$

$$P(n_i^B(t+\delta t)=n_i^B(t)+1)=\frac{\lambda}{N}\sum_{j=1}^{N} n_j^B\delta t, \qquad (5)$$

where the first equation is the probability of migration from site i and the latter that of migration to site i. The resulting model can therefore be described as quadratic autocatalysis with random mixing of B particles between cells. In what follows the volume of each site is taken to be $\Omega=1$, where the total system volume is then N, the reaction rate $K=\kappa$, and $n_{A0}=\alpha_0$.

Consider the evolution of the average reactant levels

$$\langle n_A\rangle\equiv\frac{1}{N}\sum_{i=1}^{N} n_i^A \quad\text{and}\quad \langle n_B\rangle\equiv\frac{1}{N}\sum_{i=1}^{N} n_i^B.$$

Since we have set $\Omega=1$, $\langle n_A\rangle$ and $\langle n_B\rangle$ are dimensionless quantities corresponding to the densities α and β, respectively. Figure 4 shows these average reactant levels for typical realizations of the spatial process at two mixing rates. The results show that for small mixing rate $\lambda=0.01$ the reactive state is unstable just as in the nonspatial model. However, a moderate mixing rate $\lambda=1$ stabilizes the reactive state.

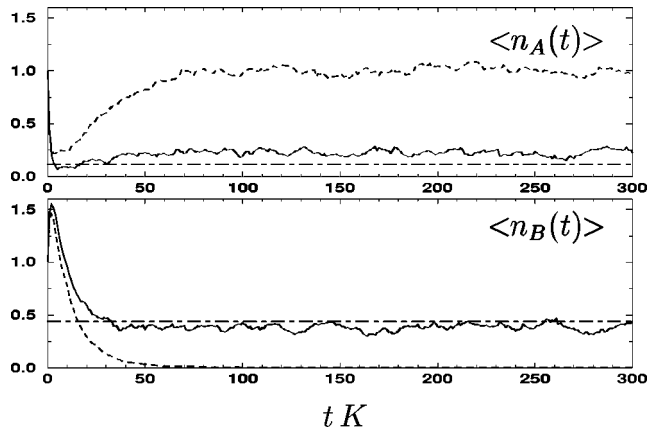

FIG. 4. Simulation of spatial system: The top graph shows typical realizations of the average density $\langle n_A(t)\rangle$ from the stochastic spatial autocatalytic process described in Sec. II against dimensionless time tK for $\lambda=1$ (solid curve) and $\lambda=0.01$ (dashed curve). The bottom graph depicts the same information for reactant B. In each case, the dot-dashed lines show the corresponding reactant levels obtained from deterministic equilibrium (2). The parameter values are $K=1$, $\alpha_0=1$, $K_b=\nu=1/17$, and $N=500$.

Figure 5 shows equilibrium estimates of the expected average reactant levels for a range of mixing rates $\lambda\in[0,2]$. These results show that a critical minimum level of mixing is required to stabilize the reactive state. For small λ, the mixing is insufficient to stabilize the reaction against stochastic fluctuation. However, as the rate of mixing increases, at

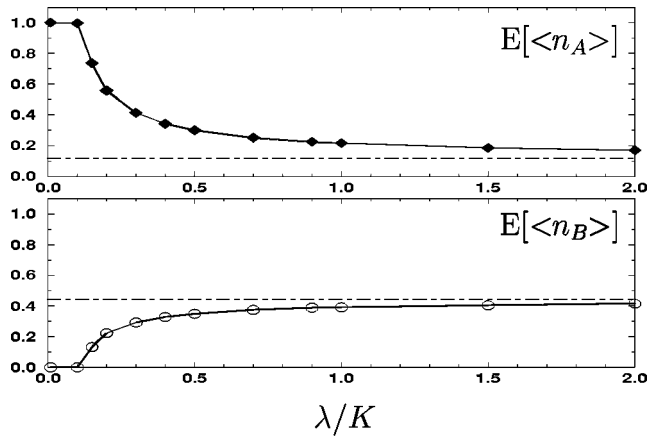

FIG. 5. Stability of reaction state: The symbols and solid curves represent estimates of $\mathrm{E}[\langle n_A\rangle]$ (diamonds) and $\mathrm{E}[\langle n_B\rangle]$ (circles) obtained from ten simulation runs, with samples collected, after a burn-in period, from $t=500,\ldots,1000$, for a range of relative values of the mixing rate λ/K. The standard errors in these estimates are approximately equal to the size of the symbols. The dot-dashed lines show the corresponding reactant levels obtained from deterministic equilibrium (2). The parameter values are $K=1$, $\alpha_0=1$, $K_b=\nu=1/17$, and $N=500$.

some critical point the reaction becomes stable across the system. Communication allows the cells to act coherently. Moreover, just above this threshold, the density of the reaction product B is considerably lower than predicted by Eq. (2), but this increases with the mixing rate to an asymptote at the level of the well-mixed deterministic system. Thus one can think of λ as controlling the effective noise level: for small noise (large λ) the system is well mixed and the mean reactant levels coincide with the deterministic nonspatial model predictions; for intermediate levels of noise the reactive state is shifted with respect to the well-mixed case; and for large noise (small λ) the reactive state is completely destabilized. Qualitatively similar results are obtained for small values of $\Omega \neq 1$.

III. SPATIAL MOMENT-CLOSURE APPROXIMATION

In order to understand better the phenomena described above, we derive analytic approximations describing the spatial system. In so doing we demonstrate the relationship between the deterministic nonspatial model and the stochastic spatial process. In particular, we construct equations describing the average reactant levels and apply the methodology developed by Keeling *et al.*, in the context of spatial models in ecology [15,16]. This approach has two principal advantages over dealing directly with the site-specific reactant levels, n_i^A and n_i^B. First, it reduces the dimensionality of the problem to be solved from $2N$ to 5 (see below). Second, even for moderate sized systems the variability of the average reactant levels will be much less than that of individual sites, and therefore the task of calculating associated statistics becomes more straightforward.

Writing the change in the level of reactant A at site i as $n_i^A(t+\delta t)=n_i^A+\delta n_i^A$, the change in the average reactant level is

$$\frac{1}{N}\sum_{i=1}^{N} n_i^A(t+\delta t)=\frac{1}{N}\sum_{i=1}^{N} n_i^A+\frac{1}{N}\sum_{i=1}^{N} \delta n_i^A.$$

Using the transition probabilities for site i as defined in Eqs. (3–5), conditional on the state of the system at time t being $n=\{(n_1^A,\ldots,n_N^A)^T,(n_1^B,\ldots,n_N^B)^T\}$ the expected change during a small time interval $(t,t+\delta t)$ is then given by

$$\mathrm{E}\left[\frac{1}{N}\sum_{i=1}^{N} n_i^A(t+\delta t)\,|\,n(t)=n\right]$$
$$=\frac{1}{N}\sum_{i=1}^{N} n_i^A+\left(-\kappa\frac{1}{N}\sum_{i=1}^{N} n_i^A n_i^B+\nu\alpha_0-\nu\frac{1}{N}\sum_{i=1}^{N} n_i^A\right)\delta t.$$

Whence evaluating expectations $\mathrm{E}[\cdot]$ at time t, and rearranging, leads to

$$\mathrm{E}\left[\frac{1}{N}\sum_{i=1}^{N} n_i^A(t+\delta t)\right]-\mathrm{E}\left[\frac{1}{N}\sum_{i=1}^{N} n_i^A\right]$$
$$=\left(-\kappa\mathrm{E}\left[\frac{1}{N}\sum_{i=1}^{N} n_i^A n_i^B\right]+\nu\alpha_0-\nu\mathrm{E}\left[\frac{1}{N}\sum_{i=1}^{N} n_i^A\right]\right)\delta t.$$

For any random variable z_i associated with site i, write the spatial average

$$\langle z\rangle=\frac{1}{N}\sum_{i=1}^{N} z_i.$$

Then taking the limit $\delta t\to 0$ yields

$$\frac{d}{dt}\mathrm{E}[\langle n_A\rangle]=-\kappa\mathrm{E}[\langle n_A n_B\rangle]+\nu\alpha_0-\nu\mathrm{E}[\langle n_A\rangle]. \qquad (6)$$

The equation describing the evolution of the average level of reactant B, namely,

$$\frac{d}{dt}\mathrm{E}[\langle n_B\rangle]=\kappa\mathrm{E}[\langle n_A n_B\rangle]-(K_b+\nu)\mathrm{E}[\langle n_B\rangle] \qquad (7)$$

is obtained in a similar manner. The difficulty with Eqs. (6) and (7) is that they depend on the second-order term $\mathrm{E}[\langle n_A n_B\rangle]$. In order to close this system of equations one may choose to approximate this term as a function of the first-order terms $\mathrm{E}[\langle n_A\rangle]$ and $\mathrm{E}[\langle n_B\rangle]$. This problem is characteristic of nonlinear stochastic processes, and a number of closure approximations exist. Broadly speaking, they may be classified into three types, namely, moment closure, cumulant truncation, and spatial moment closure. In each case, higher-order terms such as $\mathrm{E}[\langle n_A n_B\rangle]$ are replaced by functions of lower-order terms (i.e. $\mathrm{E}[\langle n_A\rangle]$ and $\mathrm{E}[\langle n_B\rangle]$). Moment closure [17,18] achieves this by making some ansatz which determines the functional dependence; for example that the process is Gaussian [19]. An alternative approach is cumulant truncation [20,21] whereby the moment equations are reexpressed in terms of cumulants (see, e.g., Ref. [22]) and higher-order cumulants are assumed to be zero. For example, second-order cumulant truncation sets third- and higher-order cumulants to zero and thus corresponds to moment closure by the normal approximation. The complexities involved in such methods are highlighted by the fact that higher-order truncation does not necessarily improve the accuracy of the approximation [23]. In spatial systems, isotropy is often invoked and boundary (finite-size) effects are ignored. Attention then focuses entirely on spatial moments, and to eliminate higher-order terms one either makes a distributional assumption [15,16] or appeals to the spatial connectedness of the system [24–26]. We note that closely related cluster approximations have been applied in chemical physics [27] and the study of nonideal gases [28].

For the model considered here, the simplest moment-closure scheme is the *mean-field* approximation, which as-

sumes that there is no correlation between the mean numbers of A and B particles, that is, $\mathrm{E}[\langle n_A n_B\rangle]=\mathrm{E}[\langle n_A\rangle]\mathrm{E}[\langle n_B\rangle]$. This recovers the deterministic system (1) on substituting $\alpha=\mathrm{E}[\langle n_A\rangle]$ and $\beta=\mathrm{E}[\langle n_B\rangle]$. However, to understand the effect of spatial heterogeneity, second-order terms must be considered. The following equations describing the evolution of $\mathrm{E}[\langle n_A n_B\rangle]$, $\mathrm{E}[\langle n_A^2\rangle]$, and $\mathrm{E}[\langle n_B^2\rangle]$ can be developed along similar lines to Eq. (6):

$$\frac{d}{dt}\mathrm{E}[\langle n_A n_B\rangle]=(\mathrm{E}[\langle n_A^2 n_B\rangle]-\mathrm{E}[\langle n_A n_B^2\rangle])\kappa - (\kappa+K_b+2\nu+\lambda)\mathrm{E}[\langle n_A n_B\rangle] + \lambda\mathrm{E}[\langle n_A\rangle\langle n_B\rangle]+\nu\alpha_0\mathrm{E}[\langle n_B\rangle], \quad (8)$$

$$\frac{d}{dt}\mathrm{E}[\langle n_A^2\rangle]=-2\kappa\mathrm{E}[\langle n_A^2 n_B\rangle]+(2\alpha_0+1)\nu\mathrm{E}[\langle n_A\rangle] - 2\nu\mathrm{E}[\langle n_A^2\rangle]+\kappa\mathrm{E}[\langle n_A n_B\rangle]+\nu\alpha_0,$$

$$\frac{d}{dt}\mathrm{E}[\langle n_B^2\rangle]=2\kappa\mathrm{E}[\langle n_A n_B^2\rangle]-2(K_b+\nu+\lambda)\mathrm{E}[\langle n_B^2\rangle] + 2\lambda\mathrm{E}[\langle n_B\rangle^2]+\kappa\mathrm{E}[\langle n_A n_B\rangle] + (K_b+\nu+2\lambda)\mathrm{E}[\langle n_B\rangle].$$

Equations (6)–(8) contain two kinds of higher-order terms which must be removed to close the system. First, $\mathrm{E}[\langle n_A\rangle\langle n_B\rangle]$ and $\mathrm{E}[\langle n_B\rangle^2]$ are second-order moments of $\langle n_A\rangle$ and $\langle n_B\rangle$ with respect to the distribution of state variables at time t. In the following, we ignore fluctuations in these quantities (also in $\mathrm{E}[\langle n_A n_B\rangle]$, $\mathrm{E}[\langle n_A^2\rangle]$, and $\mathrm{E}[\langle n_B^2\rangle]$), so $\mathrm{E}[\langle n_A\rangle\langle n_B\rangle]=\mathrm{E}[\langle n_A\rangle]\mathrm{E}[\langle n_B\rangle]$, and $\mathrm{E}[\langle n_B\rangle^2]=\mathrm{E}[\langle n_B\rangle]^2$. It is anticipated that this approximation will be valid for large system size N. Second, $\mathrm{E}[\langle n_A^2 n_B\rangle]$ and $\mathrm{E}[\langle n_A^2 n_B\rangle]$ are third-order terms with respect to the spatial distribution. These terms will be approximated by functions of the first- and second-order quantities $\mathrm{E}[\langle n_A\rangle]$, $\mathrm{E}[\langle n_B\rangle]$, $\mathrm{E}[\langle n_A n_B\rangle]$, $\mathrm{E}[\langle n_A^2\rangle]$, and $\mathrm{E}[\langle n_B^2\rangle]$. Two forms of closure (functional forms), stochastic linearization and the log-normal approximation are now considered.

A. Stochastic linearization

In this method any terms that are nonlinear in *stochastic* variables are removed by replacing carefully selected expressions with their expectations [29]. Equations describing the evolution of the moments of the resulting linear model are closed, and thus can be used to approximate the original nonlinear process. In the present case, modifying the site-specific autocatalytic reaction rate in Eq. (4) to $K\mathrm{E}[\langle n_A n_B\rangle]$, that is, the expectation of the average reaction rate over all sites, leads to a closed system of equations, which can be obtained from Eqs. (6)–(8) by substituting

$$\mathrm{E}[\langle n_A^2 n_B\rangle]=\mathrm{E}[\langle n_A\rangle]\mathrm{E}[\langle n_A n_B\rangle] \quad \text{and}$$

$$\mathrm{E}[\langle n_A n_B^2\rangle]=\mathrm{E}[\langle n_A n_B\rangle]\mathrm{E}[\langle n_B\rangle]. \quad (9)$$

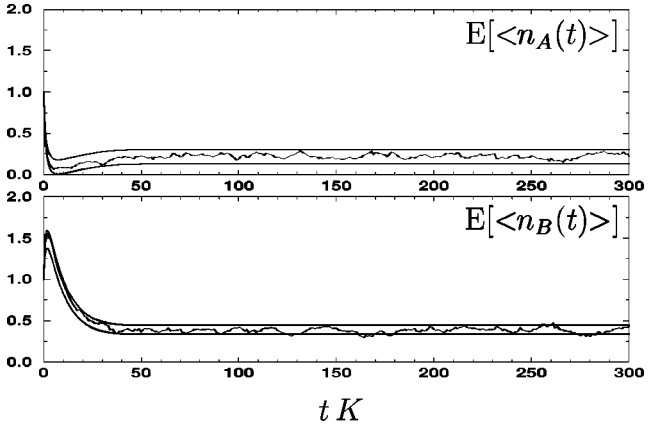

FIG. 6. Stochastic linearization: Large mixing rate $\lambda=1$. The top graph shows a typical realization (also shown in Fig. 4) of the average density $\langle n_A(t)\rangle$ against rescaled time tK from the stochastic spatial autocatalytic process (jagged line). The confidence interval $\mathrm{E}[\langle n_A\rangle]\pm 1.96\sigma_A$ (solid curves) is obtained by numerical solution of Eqs. (6)–(8) under the stochastic linearization approximation (9). The bottom graph depicts the same information for reactant B. In each case the parameter values are $K=1$, $\alpha_0=1$, $K_b=\nu=1/17$, and $N=500$.

Under this approximation the covariance $C_{AB}=\mathrm{E}[\langle n_A n_B\rangle]-\mathrm{E}[\langle n_A\rangle]\mathrm{E}[\langle n_B\rangle]$ obeys the equation

$$\frac{d}{dt}C_{AB}(t)=-(\lambda+\kappa+K_b+2\nu)C_{AB}(t) - \kappa\mathrm{E}[\langle n_A(t)\rangle]\mathrm{E}[\langle n_B(t)\rangle], \quad (10)$$

which may be solved by Fourier transformation and application of the convolution theorem to give

$$C_{AB}(t)=-\kappa\int_0^\infty \mathrm{E}[\langle n_A(t-T)\rangle]\mathrm{E}[\langle n_B(t-T)\rangle] \times e^{-(\lambda+\kappa+K_b+2\nu)T}\,dT. \quad (11)$$

Keeling *et al.* [15] obtain a similar result in the context of predator-prey models, suggesting that it reveals the form of delay equation which would account for spatial heterogeneity in the system. Expression (11) also shows that $C_{AB}\leqslant 0$, so the reaction rate in the spatial model, $K\mathrm{E}[\langle n_A n_B\rangle]=K\mathrm{E}[\langle n_A\rangle]\mathrm{E}[\langle n_B\rangle]+KC_{AB}$, is typically lower than that of the mean-field (deterministic) model $K\mathrm{E}[\langle n_A\rangle]\mathrm{E}[\langle n_B\rangle]$. The degree of negative correlation quantifies the local depletion of reactants in the spatial system. Further insight comes from examining the steady state solution of the stochastic linearization (6), (7), and (10) for the large mixing limit, $\lambda\to\infty$, where the covariance C_{AB} becomes zero and $\mathrm{E}[\langle n_A\rangle]$ and $\mathrm{E}[\langle n_B\rangle]$ correspond to the reactive state of the deterministic system (2). Thus a large degree of mixing reduces the correlations between reactants, reflecting the associated breakdown of spatial structure.

Figure 6 shows the results of numerical solution of the stochastic linearization approximation together with a typical realization of the full stochastic process, shown in Fig. 4, for

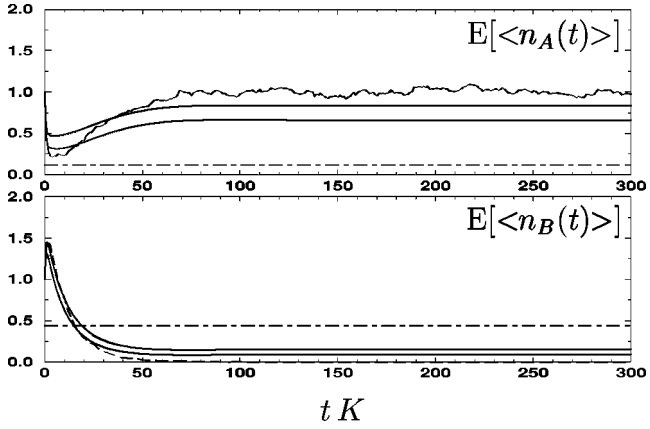

FIG. 7. Stochastic linearization: As in Fig. 6 but for small mixing rate $\lambda = 0.01$. The reactive state (α_1, β_1) of the deterministic system (1) is also shown (dot-dashed lines).

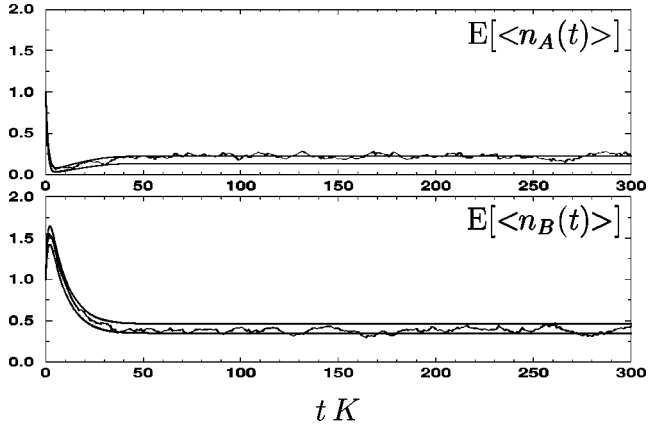

FIG. 8. Log-normal approximation: Large mixing rate $\lambda = 1$. The top graph shows a typical realization of the average density $\langle n_A(t) \rangle$ against re-scaled time tK (jagged line) as shown in Fig. 6. The confidence interval $\mathrm{E}[\langle n_A \rangle] \pm 1.96\sigma_A$ (solid curves) is obtained by numerical solution of Eqs. (6)–(8) under the log-normal approximation (12). The bottom graph depicts the same information for reactant *B*. In each case the parameter values are $K = 1$, $\alpha_0 = 1$, $K_b = \nu = 1/17$, and $N = 500$.

moderate mixing rate $\lambda = 1$. The confidence intervals shown are based on the standard errors

$$\sigma_A = \sqrt{\mathrm{E}[\langle n_A^2 \rangle] - \mathrm{E}[\langle n_A \rangle]\mathrm{E}[\langle n_A \rangle]}/\sqrt{N},$$

$$\sigma_B = \sqrt{\mathrm{E}[\langle n_B^2 \rangle] - \mathrm{E}[\langle n_B \rangle]\mathrm{E}[\langle n_B \rangle]}/\sqrt{N},$$

and the results show good agreement between simulation and approximation. Moreover, the reactant levels are close to those of the reactive state (α_1, β_1) of the deterministic system (1). In contrast, the situation shown in Fig. 7 with $\lambda = 0.01$ demonstrates that the stochastic linearization approximation breaks down for low mixing rates. In this regime, Fig. 4 shows the reactive state of spatial stochastic process to be unstable, with the system settling down to the unreactive state after a short transient phase. However, stochastic linearization predicts that the steady state reactant levels will shift compared with the case of perfect mixing, but that the reactive state will remain stable. Such failings motivate the application of an alternative approximation.

B. Log-normal approximation

An alternative to stochastic linearization is to make some assumption concerning the distribution of reactant levels over sites. A possible choice is the Gaussian distribution, but in the low mixing regime, the average level of reactant *B* tends to zero, suggesting that this or any other symmetric distribution would be a poor approximation. A nonsymmetric alternative is to assume a log-normal distribution of reactant levels over sites. As shown in the Appendix, this enables the third-order terms in Eqs. (6)–(8) to be approximated by

$$\mathrm{E}[\langle n_A^2 n_B \rangle] = \frac{\mathrm{E}[\langle n_A^2 \rangle]\mathrm{E}[\langle n_A n_B \rangle]^2}{\mathrm{E}[\langle n_A \rangle]^2 \mathrm{E}[\langle n_B \rangle]},$$

$$\mathrm{E}[\langle n_A n_B^2 \rangle] = \frac{\mathrm{E}[\langle n_B^2 \rangle]\mathrm{E}[\langle n_A n_B \rangle]^2}{\mathrm{E}[\langle n_B \rangle]^2 \mathrm{E}[\langle n_A \rangle]}. \tag{12}$$

Although the resulting moment evolution equations are more complex than for those associated with stochastic linearization, they nonetheless afford analytic insight. In the large mixing limit, $\lambda \to \infty$, these equations admit to a steady state solution

$$\mathrm{E}[\langle n_A \rangle] = \mathrm{E}[\langle n_A^2 \rangle] - \mathrm{E}[\langle n_A \rangle]^2 = (K_b + \nu)/K,$$

$$\mathrm{E}[\langle n_B \rangle] = \mathrm{E}[\langle n_B^2 \rangle] - \mathrm{E}[\langle n_B \rangle]^2 = \frac{\nu(\alpha_0 K - K_b - \nu)}{[\kappa(K_b + \nu)]},$$

$$C_{AB} = 0, \tag{13}$$

which corresponds to a Poisson-like distribution about the deterministic reactive state (2). To first order as $\lambda \to \infty$, the evolution equation for the correlation C_{AB} becomes

$$\frac{d}{dt} C_{AB}(t) = -\lambda C_{AB}(t).$$

Thus, in this limit the correlation tends to zero exponentially, as mixing breaks down spatial heterogeneity. Furthermore, this equation suggests that for $\lambda \to \infty$ the steady state (13) is an attracting state: this conjecture is supported by the numerical solution of the log-normal approximation to the moment evolution equations for $\lambda = 1$, and these results, shown in Fig. 8, also demonstrate the accuracy of the log-normal approximation.

A second steady state of the log-normal approximation, valid for all λ, is

$$\mathrm{E}[\langle n_A \rangle] = \alpha_0, \quad \mathrm{E}[\langle n_A^2 \rangle] - \mathrm{E}[\langle n_A \rangle]^2 = \alpha_0,$$

$$\mathrm{E}[\langle n_B \rangle] = 0, \quad \mathrm{E}[\langle n_B^2 \rangle] - \mathrm{E}[\langle n_B \rangle]^2 = 0,$$

$$C_{AB} = 0, \tag{14}$$

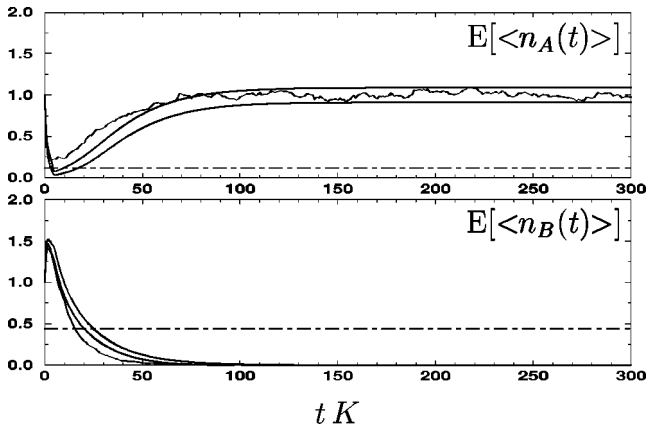

FIG. 9. Log-normal approximation: As in Fig. 8 but for small mixing rate $\lambda = 0.01$. The reactive state (α_1, β_1) of the deterministic system (1) is also shown (dot-dashed lines).

which is a Poisson-like distribution whose mean corresponds to the unreactive state of the deterministic system. Although we have been unable to determine the relative stability of the reactive [Eq. (13)] and unreactive [Eq. (14)] states of the log-normal approximation analytically, Fig. 9 demonstrates that for $\lambda = 0.01$ the unreactive state (14) is asymptotically stable in accord with results obtained by the simulation of the full stochastic model shown in Fig. 4. Thus, in contrast to stochastic linearization, the log-normal approximation is able to predict the transition to the unreactive state seen at low levels of mixing.

Figure 10 compares the log-normal approximation with the simulation results of Fig. 5. The log-normal approximation is quantitatively correct at the extremes of mixing and no mixing, and although it is less accurate, it still captures the qualitative behavior at intermediate levels of λ. As we have seen in the limit $\lambda \to \infty$, the spatial system becomes well mixed, and therefore corresponds to the nonspatial system with volume $\Omega = N$. The results of Figs. 2 and 10 imply that for small systems ($N < 50$) the reactive state will be unstable for all λ, and the log-normal approximation will break down, as is confirmed by direct simulation. This is related to the fact, noted below Eqs. (8), that the moment-closure schemes are expected to be most accurate for large N. This is because we only consider the evolution of the expected values of quantities describing the spatial distribution (i.e., $\mathrm{E}[\langle n_A \rangle]$, $\mathrm{E}[\langle n_B \rangle]$, etc.), neglecting any fluctuations between realizations of the process.

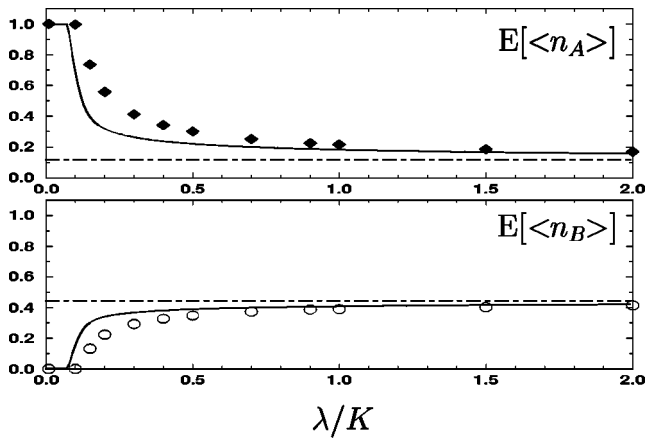

FIG. 10. Stability of reaction state: The solid lines show the asymptotic values of $\mathrm{E}[\langle n_A \rangle]$ and $\mathrm{E}[\langle n_B \rangle]$ (as indicated) obtained from the solution of the log-normal approximation for a range of relative mixing rates λ/K. The symbols represent estimates of $\mathrm{E}[\langle n_A \rangle]$ (diamonds) and $\mathrm{E}[\langle n_B \rangle]$ (circles) obtained from ten simulation runs, with samples collected, after a burn-in period, from $t = 500, \ldots, 1000$. The standard errors in these estimates are approximately equal to the size of the symbols. The parameter values are $K = 1$, $\alpha_0 = 1$, $K_b = \nu = 1/17$, and $N = 500$.

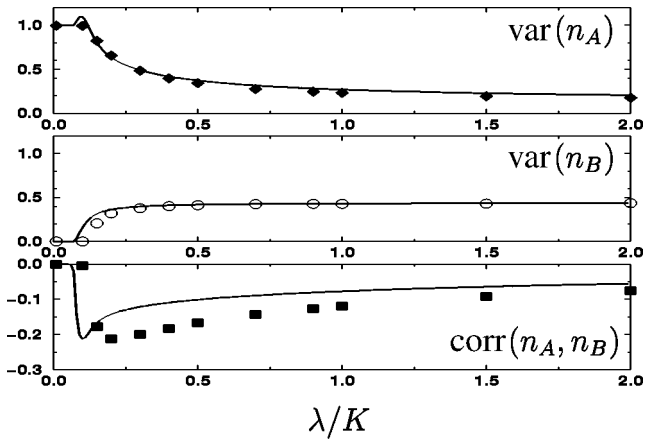

FIG. 11. Stability of reaction state: The solid lines show the asymptotic values of $\mathrm{Var}(n_A) = \mathrm{E}[\langle n_A^2 \rangle] - \mathrm{E}[\langle n_A \rangle]^2$, $\mathrm{var}(n_B) = \mathrm{E}[\langle n_B^2 \rangle] - \mathrm{E}[\langle n_B \rangle]^2$, and the normalized correlation $\mathrm{corr}(n_A, n_B) = C_{AB} / \sqrt{\mathrm{var}(n_A)\mathrm{var}(n_B)}$ (as indicated) obtained from the solution of the log-normal approximation for a range of values of the relative mixing rate λ/K. The symbols represent estimates of $\mathrm{E}[\mathrm{var}(n_A)]$ (diamonds), $\mathrm{E}[\mathrm{var}(n_B)]$ (circles), and $\mathrm{E}[\mathrm{corr}(n_A, n_B)]$ (squares) obtained from ten simulation runs, with samples collected after a burn-in period from $t = 500, \ldots, 1000$. The standard errors in these estimates are approximately equal to the size of the symbols. The parameter values are $K = 1$, $\alpha_0 = 1$, $K_b = \nu = 1/17$, and $N = 500$.

Figure 11 shows the corresponding asymptotic behavior of the covariance and variances in reactant levels across the system for a range of mixing rates. The data shown are from the simulations and solutions to the log-normal approximation used in Fig. 10. The reactants are maximally separated, and thus spatial heterogeneity is at its greatest, at the critical mixing rate where the reaction state becomes stable (unstable). For larger mixing rates, the correlation increases with λ.

IV. DISCUSSION

A living cell is an open system, which can communicate with environments by transferring chemical signals and energy. Enzymatic reactions in living cells are confined to very small spatial volumes. Moreover, these reactions are subject to strong thermal fluctuations inside the cells due to a flow of energy [14], and these conditions can lead to qualitative changes in the kinetics of enzymatic reactions in comparison with high-density well-mixed conditions. For example, co-

herent dynamics can form between substrates and enzymes when the reaction takes place in small volumes [14,30–32]. Furthermore, our results suggest that without sufficient communication between cells, certain biochemical reactions might be unstable with respect to thermal fluctuations. It would also be interesting to study the effects of within-cell spatial heterogeneity. In living cells, a large number of enzymatic reactions are networked in complicated ways, and are coupled to thousands of substrates. Pathways can be unidirectional, reversible, branched, or cyclic, and there are many different types of inhibition and activation [33]. In the postgenome era, these complex networks can be reconstructed based on genomic data. Unsurprisingly, the purposes and functions of complex biochemical networks, in particular, spatiotemporal self-organization behavior, have attracted much attention [34,35]. For enzymatic reactions, various mechanisms may lead to spatiotemporal behavior [36]. Autocatalysis represents a class of reactions of great importance to living cells and has been much studied in nonspatial contexts [2,3,5,6]. Togashi and Kaneko [37] show that stochastic fluctuations and discreteness in molecular numbers lead to transitions between states in a nonspatial autocatalytic system. The stochastic spatiotemporal autocatalytic process studied in this work can be considered a generic model for studying spatiotemporal behavior in biochemical reactions. We note that Velikanov and Kapral [38] study the propagation of traveling wave fronts in a spatially explicit discrete time (Markov chain) model of quadratic autocatalysis. Using a perturbation technique, which systematically accounts for spatial correlations, they show that the wave front velocity of the stochastic system is lower than that predicted by a mean-field analysis which ignores such correlations. Moreover, as the diffusion coefficient increases, spatial correlations are minimized and the discrepancy reduced. The phenomenon is analogous to the effect of finite mixing on the stability of the reactive state explored in the current paper. The model studied here was amenable to a spatial moment-closure approximation which compared favorably with simulations of the full stochastic process; these results demonstrate the utility of order parameters, such as the spatial averages considered here, in studying system behavior. Our investigations clearly show how internal fluctuations, small volumes, and heterogeneity affect the kinetics of the quadratic catalytic system.

In the nonspatial system at low volumes, the reactive state of the autocatalytic process is unstable to internal stochastic fluctuations. The spatial model shows that such unstable components can be linked together, via random exchange of reactants, to form a system in which the reaction is stable. For large mixing rate ($\lambda \to \infty$), the spatial system with N components behaves like a nonspatial system with volume N, but for finite mixing rate this effective volume is less than N. Thus, finite mixing generates spatial heterogeneity (correlation) which destabilizes the system with respect to a perfectly mixed system of the same volume, and there is a critical level of exchange (mixing) below which the reaction is unstable. Conversely, at the level of the cell, finite mixing stabilizes the reaction kinetics by forming a system whose effective volume is much greater than any individual cell. In conclusion, our results suggest that autocatalytic reaction kinetics may only be stable in cellular systems in which a number of cells are able to exchange reactants via some transport process. Perhaps such phenomena influenced evolution by favoring the persistence of aggregations of multiple cells over those of solitary individuals.

ACKNOWLEDGMENTS

The authors would like to thank the BBSRC and EPSRC (U.K.) for their financial support under Grant No. 78/MMI09712. In addition, G.M. and J.L. gratefully acknowledge the support of the Scottish Executive Environment and Rural Affairs Department.

APPENDIX: LOG-NORMAL APPROXIMATION

If the reactant levels n_A and n_B are log-normally distributed over sites, then $y_1 = \ln n_A$ and $y_2 = \ln n_B$ are joint normal with the moment generating function [22]

$$\begin{aligned} M(\theta_1,\theta_2) &\equiv \mathrm{E}[\langle \exp\{\theta_1 y_1 + \theta_2 y_2\}\rangle] \\ &= \exp\{\kappa_{10}\theta_1 + \kappa_{01}\theta_2 + \kappa_{20}\theta_1^2/2 \\ &\quad + \kappa_{11}\theta_1\theta_2 + \kappa_{02}\theta_2^2/2\}, \end{aligned}$$

where $\mathrm{E}[\langle\cdot\rangle]$ denotes the expectation over distributions in space and time, and

$$\kappa_{10} = 2\ln(\mathrm{E}[\langle n_A\rangle]) - \ln(\mathrm{E}[\langle n_A^2\rangle])/2,$$

$$\kappa_{01} = 2\ln(\mathrm{E}[\langle n_B\rangle]) - \ln(\mathrm{E}[\langle n_B^2\rangle])/2$$

$$\kappa_{20} = \ln(\mathrm{E}[\langle n_A^2\rangle]) - 2\ln(\mathrm{E}[\langle n_A\rangle]),$$

$$\kappa_{02} = \ln(\mathrm{E}[\langle n_B^2\rangle]) - 2\ln(\mathrm{E}[\langle n_B\rangle]),$$

$$\kappa_{11} = \ln(\mathrm{E}[\langle n_A n_B\rangle]) - (\kappa_{20}+\kappa_{02})/2 - \kappa_{10} - \kappa_{01}.$$

For an appropriate choice of θ_1 and θ_2 expressions for the higher-order terms, $\mathrm{E}[\langle n_A^2 n_B\rangle]$ and $\mathrm{E}[\langle n_A n_B^2\rangle]$ are obtained from

$$\mathrm{E}[\langle n_A^{\theta_1} n_B^{\theta_2}\rangle] = \langle[\exp\{\theta_1 y_1 + \theta_2 y_2\}]\rangle = M(\theta_1,\theta_2).$$

For example, setting $\theta_1 = 2$ and $\theta_2 = 1$ yields

$$\begin{aligned} \mathrm{E}[\langle n_A^2 n_B\rangle] &= M(2,1) \\ &= \exp\{2\kappa_{10} + \kappa_{01} + 2\kappa_{20} + 2\kappa_{11} + \kappa_{02}/2\}, \end{aligned}$$

which simplifies to

$$\mathrm{E}[\langle n_A^2 n_B\rangle] = \frac{\mathrm{E}[\langle n_A^2\rangle]\mathrm{E}[\langle n_A n_B\rangle]^2}{\mathrm{E}[\langle n_A\rangle]^2 \mathrm{E}[\langle n_B\rangle]}.$$

The resulting expressions (12) can then be used to close the system of moment evolution equations (6)–(8).

[1] M.A. Gibson and J. Bruck, in *Computational Modeling of Genetic and Biochemical Networks*, edited by J. M. Bower and H. Bolouri (Massachusetts Institute of Technology Press, Cambridge, MA, 2001).
[2] P. Gray and S.K. Scott, Chem. Eng. Sci. **39**, 1087 (1984).
[3] P. Gray and S.K. Scott, *Chemical Oscillations and Instabilities* (Oxford University Press, Oxford, 1990).
[4] A. Goldbeter, *Biochemical Oscillations and Cellular Rhythms: The Molecular Basis of Periodic and Chaotic Behaviour* (Cambridge University Press, Cambridge, 1996).
[5] J. Liu and J.W. Crawford, Proc. R. Soc. London, Ser. A **453**, 1195 (1997).
[6] J. Liu and S.K. Scott, J. Chem. Phys. **94**, 4416 (1991).
[7] W. Horsthemke and R. Lefever, *Noise-induced Transitions* (Springer-Verlag, Berlin, 1984).
[8] G. Marion, X. Mao, E. Renshaw, and J. Liu (unpublished).
[9] N.G. Van Kampen, *Stochastic Processes in Physics and Chemistry* (North Holland, Amsterdam, 1992).
[10] E. Renshaw, *Modelling Biological Populations in Space and Time* (Cambridge University Press, Cambridge, 1991).
[11] M. Malek Mansour, C. Van den Broeck, G. Nicolis, and J.W. Turner, Ann. Phys. (N.Y.) **131**, 283 (1981).
[12] K. Kitahara, Adv. Chem. Phys. **29**, 85 (1975).
[13] Q. Zheng, J. Ross, K.L.C. Hunt, and P.M. Hunt, J. Chem. Phys. **96**, 630 (1992).
[14] B. Hess and A.S. Mikhailov, Science **264**, 223 (1994).
[15] M.J. Keeling, H.B. Wilson, and S.W. Pacala, Science **290**, 1758 (2000).
[16] M.J. Keeling, J. Anim. Ecol. **69**, 725 (2000).
[17] V. Isham, Math. Biosci. **107**, 209 (1991).
[18] G. Marion, E. Renshaw, and G. Gibson, Theor Popul. Biol. **57**, 197 (2000).
[19] P. Whittle, J. R. Stat. Soc. Ser. B. Methodol. **19**, 266 (1957).
[20] J.H. Matis, T.R. Kiffe, and P.R. Parthasarathy, Theor Popul. Biol. **53**, 16 (1998).
[21] J.H. Matis and T.R. Kiffe, *Stochastic Population Models: Lecture Notes in Statistics 145* (Springer, New York, 2000).
[22] M.G. Kendall, *Kendall's Advanced Theory of Statistics* (Edward Arnold, London, 1994).
[23] E. Renshaw, Math. Biosci. **168**, 57 (1999).
[24] S.A. Levin and R. Durrett, Philos. Trans. R. Soc. London, Ser. B **351**, 1615 (1996).
[25] B. Bolker and S.W. Pacala, Theor. Popul. Biol. **52**, 179 (1997).
[26] J.A.N. Filipe and G.J. Gibson, Philos. Trans. R. Soc. London, Ser. B **353**, 2153 (1998).
[27] E. Ben-Naim and P.L. Krapivsky, J. Phys. A **27**, L481 (1994).
[28] A. Kostyuk, M. Gorenstein, H. Stocker, and W. Grenier, Phys. Rev. C **63**, 044901 (2001).
[29] W.Y. Tan and H. Hsu, Stat. Med. **8**, 121 (1989).
[30] B. Hess and A.S. Mikhailov, Biophys. Chem. **58**, 365 (1996).
[31] P. Stange, A.S. Mikhailov, and B. Hess, J. Phys. Chem. B **103**, 6111 (1999).
[32] P. Stange, A.S. Mikhailov, and B. Hess, J. Phys. Chem. B **104**, 1844 (2000).
[33] L. Stryer, *Biochemistry* (Freeman, New York, 1991).
[34] A.C. Moller, M.J.B. Hauser, and L.F. Olsen, Biophys. Chem. **72**, 63 (1998).
[35] M.J. Berridge, Nature (London) **386**, 759 (1997).
[36] I. Schreiber, Y.F. Hung, and J. Ross, J. Phys. Chem. **100**, 8556 (1996).
[37] Y. Togashi and K. Kaneko, Phys. Rev. Lett. **86**, 2459 (2001).
[38] M.V. Velikanov and R. Kapral, J. Chem. Phys. **110**, 109 (1999).